Thermal analysis of meso-scale high-temperature Borehole Thermal Energy Storage (BTES) systems with varying operational cycles

Murat Aydin	University of Kiel	murat.aydin@ifg.uni-kiel.de
Bo Wang	University of Kiel	bo.wang@ifg.uni-kiel.de
Jens Lingenauer	University of Kiel	stu116000@mail.uni-kiel.de
Sebastian Bauer	University of Kiel	sebastian.bauer@ifg.uni-kiel.de

Peer review status:

This is a non-peer-reviewed preprint submitted to EarthArXiv.

Thermal analysis of meso-scale high-temperature Borehole Thermal Energy Storage (BTES) systems with varying operational cycles

Murat Aydin*, Bo Wang, Jens Lingenauer, and Sebastian Bauer

*Institute of Geosciences, University of Kiel, Kiel, Germany (murat.aydin@ifg.uni-kiel.de)

Abstract

High temperature and short-term subsurface heat storage using BTES is a promising option and an emerging technology for increasing the fraction of renewable energy in the heat sector and supplying stored heat at high and directly usable temperatures. Investigation of thermal interactions of multiple BHEs employed for high-temperature cyclic storage operations is required to understand the system behavior and the relevant thermal processes involved. This work therefore presents highly controlled meso-scale experiments for high temperature borehole thermal energy storage.

The experiment is set up at Kiel University, using a sand pit with two-meter depth and a volume of 37 m^3 filled with partially saturated fine sand. Five BHEs are constructed, with four positioned at the edges of a square of 0.7 m side length and the fifth one in the center. The temperatures are measured at 224 locations at varying distances and depths from the center BHE. For the tests, inflow temperatures of the BHEs were set to represent a high temperature storage system for both stationary and cyclic heat loads by using 70°C and 10-15°C inflow temperature for heating and cooling cycles, respectively. The range of the cycles was changed from 12 to 120 hours.

All BHEs were jointly operated using the same inflow temperatures, to determine the effect of their thermal interactions on the recovery factor of cyclic storage operations. Thermal interaction due to the simultaneous operation of the BHEs reduced the heat transfer rate by about 30% after 12 hours of continuous heating in the center BHE, while for the outer BHEs the heat transfer rate was reduced by approximately 24%. After about three days of continuous heating, heat transfer rates have stabilized at about 60% in the outer and 40% in the center BHE. Based on these values, a thermal recovery factor of 55% is obtained. For the cyclic heat storage experiments, similar utilization ratios were found, although average heat transfer rates for the individual BHEs increase with decreasing cycle time. Furthermore, although heat transfer rates are lower in the joint operation of the BHEs, temperatures in the sand are higher. Temperatures in the sand at 0.2 m from the center BHE increase from 30°C for individual BHE operation to 57 °C in the joint operation, thus providing higher storage temperatures.

Keywords: High Temperature Borehole Thermal Energy Storage, Borehole Heat Exchanger

Introduction

Borehole Thermal Energy Storage (BTES) is a sensible, seasonal underground thermal energy storage (TES) method. In the last years BTES have been getting more popular and started to be used widely around the world with different design and running properties because of their important advantages. These systems can reduce the mismatch between the energy demand and energy supply (Dincer & Rosen, 2011) especially in the utilization of renewable resources; therefore they can reduce the utilization rate of fossil fuel and increase the rate of renewable energies and correspondingly help to protect the environment.

For the definition of BTES different approaches can be found in literature. Early researchers Bo Nordell (1994) and Gehlin. S (2016) states that every borehole system can be identified as a BTES.

However, Sanner & Stiles (1997) give another description, they indicate a borehole array as a BTES if its seasonal heat loss is lower than the 25% of the total injected heat. Skarphagen et.al. (2019) showed also that single borehole cannot store thermal energy efficiently, and they remarked that 20-40% heat storage efficiency is not feasible to invest and therefore a single borehole can be used only for heating or cooling purposes.

BTES systems can be applied everywhere and can store larger amount of heat in underground (Sarbu & Sebarchievici, 2018) in a seasonal time scale and they can be more efficiently used for especially district heating systems (Welsch et al. 2018) through storing the summer solar energy or waste heat energy. In currently active BTES systems, for heat sources mostly solar energy is used, only a few of them use the other heat sources like industrial heat waste (Emil Nilsson, 2020). However, in the last years they started to use also other purposes, for instance Giordano, N. & Raymond, J. (2019) designed a BTES system for subarctic climate to produce heat for drinking water facilities.

BTES systems can be classified based on their storage temperature. If the storage temperature is higher than 40°C they are classified as high temperature and if the temperature is lower than 30°C they are classified as low temperature (Gehlin 2016, Skarphagen et. al. 2019). High temperature BTES can be more efficiently used in heating systems, especially without heat pumps therefore in this aspect using High Temperature Borehole Thermal Energy Storage (BTES) seems a more promising option for increasing the fraction of renewable energy (Ekmekci et al. 2024).

In performance characterization of BTES, recovery factor is generally used. To calculate the recovery factor, the extracted heat energy is divided by the injected heat energy into BTES for a cycle time. For district heating systems, the cycle time is a year, generally heat is collected from solar energy in summer and extracted in wintertime.

To date, numerous studies have investigated the BTES systems. Because BTES systems require large spaces in fields, for detailed studies generally well designed and controlled laboratories are used. Those systems are small however they can be analyzed with nondimensionalizing method (Abbas et al. (2020), Pallard et al. (2020)) and these validated models can be used for predictions to the large-scale systems Moradi et al. (2016). Furthermore, in the last years also some middle and large type BTES studies (Guo et al. (2020), Baser & McCartney (2020)) and some long-term monitoring with high frequency studies Naicker & Rees (2020) are also performed. VDI directly attributes the recovery rates to volume of the storage field, for smaller volumes (<30k m^3) 50-60% for larger volumes 80-90% can be reached VDI 4640, (2001). Similarly, some also thermal efficiency optimization studies (Bayer et al. 2014) and (Rapantova et al. 2016) carried out and it is shown that recovery factor can be increased up to 84% (Schulte, 2016).

Although numerical analyses predict always higher recovery rates, lower recovery values were reported from the working BTES systems. Generally, achieving a stable working condition takes a few years and therefore efficiency is lower than expected in the first couple of years, then after that period a stable condition is reached. Some of current BTES, Neckarsulm (Bauer et al. 2010) Anneberg (Lundh & Dalenbäck, 2008) and Drake Landing (Sibbitt et al. 2012) show the efficiency ratio between 30-50 %. Anneberg has 46% without including heat losses (Lundh & Dalenbäck, 2008). For Neckarsulm (Germany) project where 50 °C is used for heat storage recovery efficiency is around 44.8%. However, Emmaboda in the first years 37% performance was obtained, however the efficiency was increased 61% in the following years (Emil Nilsson, 2020) and (Nordell et al. 2015). In Canada in Drake Landing project, in which residential heating 52 Houses are heated up with this BTES supported heating system, five years' performances in sequence are 6%, 20%, 35%, 54%, 36%. In this project different than the like others, that BTES system is supported with a natural gas heating system and a short-term thermal energy storage existed. One of the very

early BTESs is in Lulea Store in Sweden, in the first year 11.5% recovery was obtained and in the following years 50.2%, 37.0%, 57.9% and 34.9% various recovery factors were obtained (Nordell, 1994).

In the design process of a BTES, the main target is getting maximum recovery factor, in other words recovering as much energy as possible that is injected in the charge phase. Therefore, the efficiency of a BTES system is generally defined as the recovery factor. In the injection phase the injected heat is propagated around the storage field and dissipated in the ground. For large systems heat is started to be given from the center BHEs and later to the outer BHEs and the core of the storage field can be kept always warm (Skarphagen et al, 2019), that method can be easily applied in BTES in cylindrical geometry. From the outer BHEs heat also diffuses to outside of the storage field and this causes loss of heat energy from the storage field as well as from the top surface and bottom surface. Therefore, geometry of a storage field is another important factor in achieving higher recovery factors (Ekmekci et al, 2023). Based on the charge temperature and undisturbed ground temperature and largeness of the storage field different efficiencies can be obtained.

Another important design criterion is the distance between the BHEs in the storage field. The optimum distance between the boreholes is also related to usage of the system (Reuss, M, 2015), for heating dominated system the distance should be as large as possible. However, in an underground heat storage system, distance between BHEs should be as optimum as possible based on the injection temperature, storage size, thermal properties of ground and length of charge - discharge cycles. Welsch (2019) states that efficiency is also highly related to cycle length of the charge and discharge, and it is reported that if the stored heat is not totally exploited there is not an effect of the cycle length to the efficiency. Furthermore, Lanahan & Tabares-Velasco (2017) highlights that seasonal storage works efficiently with diurnal heat storage, with this method the solar fraction can be increased.

The extracted heat energy is directly related to propagation of the heat in the ground. Therefore, an important thing in the storage system is controlling the heat propagation in the ground and minimizing the heat loss to the environment as much as possible. To decrease the heat loss the design parameters must be carefully determined. One of the important design parameters is the surface of the heat storage volume. As the minimum volume/surface area ratio can be obtained from shape of sphere, the closest and feasible applicable storage geometry is a cylindrical geometry with same depth and radius. Some systems were designed with considering these criteria (Bauer et al. 2010).

According to the literature survey given above there is not a clear consensus of the thermal performance of meso-scale BTES. Their cycle length of the charge and discharge processes have high effects on recovery factors, and there is a lack of information on this subject, and it needs a detailed investigation. Therefore, in this study thermal performance of meso-scale BTES is aimed. We built in this study a well-designed and controlled meso-scale BTES system. Numerical validation of this BTES was provided by Wang et al (2024). Here, however to see the effect of different cycle lengths, the BTES systems were run with different cycles with the same test conditions. In the methodology section, experimental test system is described, in the results section the main important results are presented and, in the discussion, and conclusion section main outputs from the study are given.

2. Methodology

The experimental setup was built up at Kiel University in a laboratory which is a single apart facility separated from main buildings. The test field in the laboratory is almost the same condition as

the outside atmosphere except having a roof and lateral covers which only provide a shading from solar insolation and protect the field from the winds, and the closed place protects the measurement systems and use long time usage for different studies. The storage field is filled with partially saturated fine sand, and it has approximately two-meter depth and a total volume of 37 m^3. For the storage medium, sand is chosen, because of its thermal properties previously known and its properties can be controlled easily. Five co-axial BHEs are constructed in the storage field, one at the middle and four are positioned at the edges of a square of 0.7 m side length. The distances between the BHEs are kept closer to see interactions in shorter time scales. The storage field and test system with control and measurement equipment are depicted in **Fig. 1**.

Installation of Boreholes

Cross-sectional view of BHEs is given also upper side of in **Fig. 1**. For grouting, packaged and easy to use grouting materials from (ThermoCem TC04, 2017) were used, all BHEs grouted on site from bottom to top to ensure not leaving air gaps in the grout. For measuring the grout temperature, temperature sensors were located inside of the grout in different depths (red point in cross-section of BHE in **Fig. 1**). Geometrical properties of the boreholes are given in **Table 1**.

Table 1. Geometrical properties of the boreholes.

Geometrical Properties of Borehole		
Inner radius of inner pipe	13.5	mm
Thickness of inner pipe	7	mm
Inner radius of outer pipe	27.7	mm
Outer pipe thickness	3.8	mm
Length of BHE 2-5	1.87	m
Length of BHE 1	1.98	m
Borehole radius	130	mm

The test system consists of a Heat Source with 4000 W and measuring tools like flowmeters, temperature sensors, pressure gauges and hydraulic balance valves. The BHEs in the storage field are connected to the heat source with high durable flexible pipes.

Circulating fluid in the systems are provided and collected in parallel to the boreholes via inlet and outlet collectors to give fluid in the same temperature to all BHEs at the same time.

To avoid the problems related to air and pressure difference in the parallel connection (Kavanaugh and Rafferty, 2014) the system was connected from bottom to top and at the highest point of the pipe connection an automatic air-purge was located. Furthermore, for supplying equal amounts of thermal energy to each single borehole the hydraulic pressure drops from individual pipes were equalized. For hydraulic pressure, the system is analyzed with the pressure drop equation:

$$\Delta P = f \frac{L}{D} \rho \frac{V^2}{2} \tag{1}$$

where ΔP is pressure drop (Pa), L is the length of the pipe (m), D is the diameter of the pipe (m), ρ density of fluid (kg/m^3) and V is the velocity of fluid (m/s).

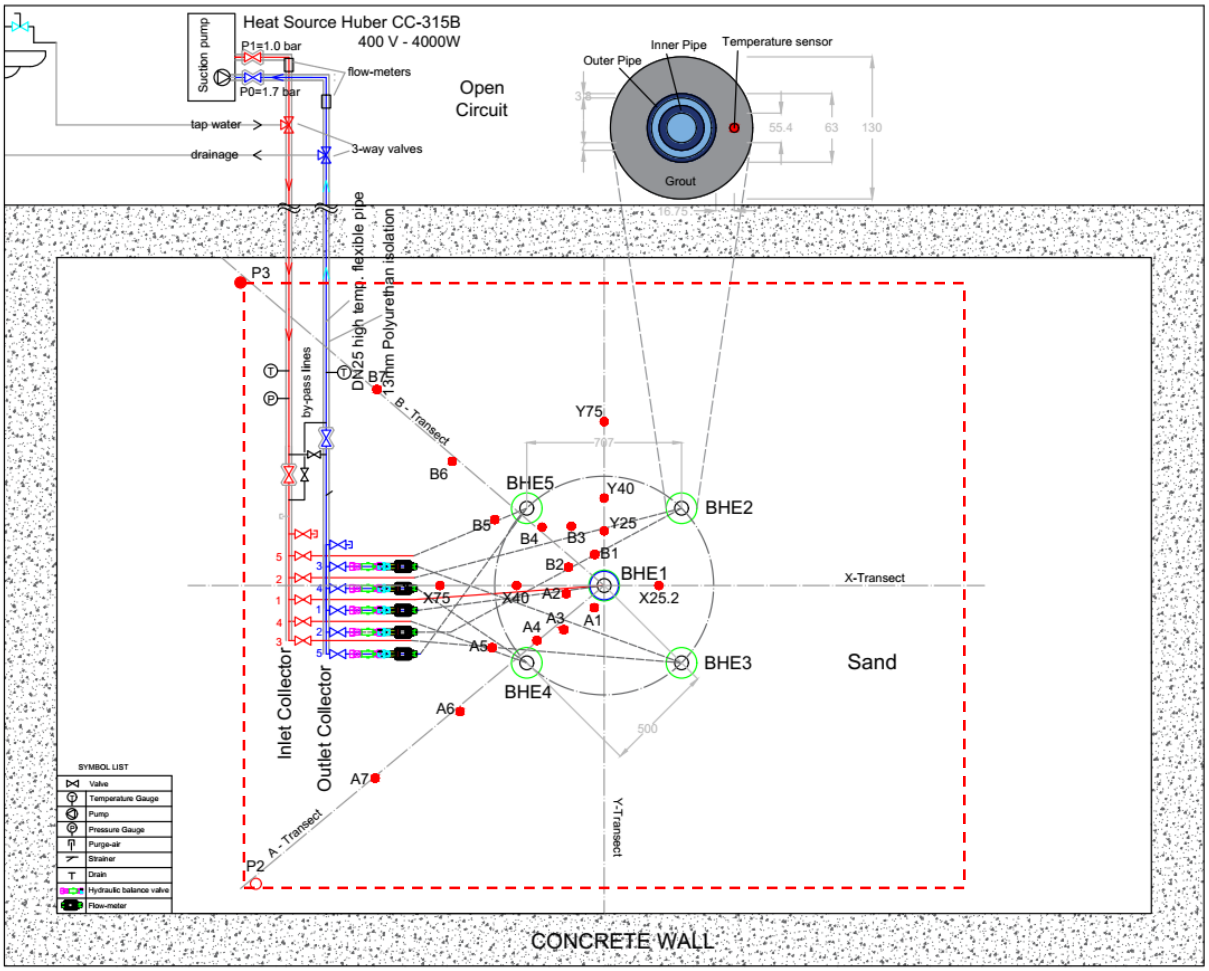

Fig. 1: View of the BHE test field.

f is the friction factor, that can be found with implicit Colebrook equation iteratively:

$$\frac{1}{\sqrt{f}} = -2\log\left(\frac{\varepsilon/D}{3.7} + \frac{2.51}{\mathrm{Re}\sqrt{f}}\right) \tag{2}$$

ε is roughness coefficient of pipes and Re is Reynolds number. Our system is an open system and pressure difference is provided from with a suction pump in the return of the heat source, inlet is open the atmosphere and the pressure is equal to P_{atm}. Hence it can be seen that $\Delta P = P_{suction} - P_{atm}$ is constant between the inlet and outlet, also as well as in the BHE loops between inlet and outlet collectors. When we use Eq.1 for the loops between inlet and outlet collectors and

$$f_x L_x V_x^2 = f_y L_y V_y^2 \tag{3}$$

if the lengths are not equal, the velocities will be also unequal. This problem was solved by keeping equal pipe lengths in all loops and beside this, for unpredictable minor changes, hydraulic balance valves were also used in the return lines. Moreover, cross connection sequence (Tichellman's parallel-circuit, Siegenthaler, J. (2011) was used in connections of the inlet and outlet pipes to the collectors (**Fig. 1**).

To reduce the heat losses from the surface of all the pipes, the surfaces were properly insulated. The top of the storage field was also insulated with mineral wool isolators and also polystyrene

foam insulators in some places where rigidness is required. With this application heat loss is minimized.

The fluid and ground temperatures of the sand are measured from 224 different locations. The ground temperature sensors are located varying distances and depths from the center BHE (**Fig. 2**). Thermal properties of materials that exist in the laboratory are given in the **Table 2**.

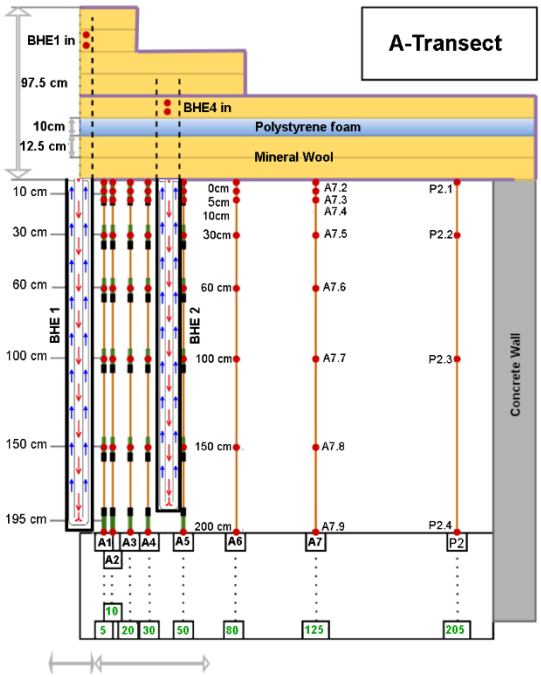

Fig. 2. Location of temperature sensors and boreholes in the A transect (Lingenauer, 2020).

For experimental tests, inflow temperatures of fluid to the BHEs were set to 70°C to represent a high temperature storage system for both stationary and cyclic heat loads. For the discharge, tap water from the city grid was used, the range of its temperature changes mainly between 10°C and 15°C.

Table 2. Thermal properties of the materials in the laboratory (Liedtke, 2019; Wang et al, 2024).

Material	Vol. Heat Capacity [kJ/(m^3.K)]	Thermal Conductivity [W/(m.K)]
Surrounding ground	2000	0.40
Concrete wall	2100	1.60
Grout-BHE	2190	3.50
Dry Sand	2019	1.50
PE pipe-BHE	1950	0.38
Mineral wool	45	0.04
Polystyrene Foam	41.3	0.04
Saturated Sand	2340	1.93
Gravel	2400	1.80
Mergel	2080	2.36

Flowrates are measured from two different flowmeters in the main line, one is in the flow direction, the other is in the return direction (**Fig. 1**). In the return line of each BHE loops flowrates are measured with magnetic-inductive flowmeters (**Table 3**).

Table 3. Properties of flowmeters, moisture and temperature sensors

Flowmeter	Measurement rage	0.05 ... 35 l/min
	Accuracy	± (0.8 % MW + 0.2 % MEW)
	Repeatability	± 0.2 % MEW
Temperature	Sensor Type	143 Typ-K
	Tolerance	0.75 %
Moisture	Sensor Type	76 SMT-100

For conversion of the data, PXI Temperature Measurement Module PXIe 4353 and PXI-Chassis PXIe-1082 from NI were used. Data recording and pre-visualization were carried out with LabVIEW from NI.

Heat Loss

3D view of the storage field is illustrated in **Fig. 3**, lateral surfaces of the storage field are surrounded by concrete walls, at top of the field an insulation layer was located for all the borehole and also at the core of the storage one more insulation layer was located to minimize the heat loss to the air.

As mentioned above, heat loss from the storage field is critically important. The heat loss occurs to the air from the top and to the surrounding ground from the lateral surfaces and from the bottom.

3. Results

After building the test system and completing essential control tests like leakage test, accuracy test of the measurements etc., real experimental tests were started. The BHEs were tested in different sequences, together and individually in different times.

Thermal characteristics of BHEs

Before starting the cyclic tests, all BHEs were tested individually to make sure that all of them have similar thermal characteristics. To ensure the same conditions for each test, two weeks waited for recovery of the field between the tests as is also recommended by Ashrae (2011) furthermore temperatures of the underground were monitored also in the recovery period. **Fig. 4** shows unit heat transfer rates of the BHEs that were obtained from the individual tests which were carried out with 70°C constant inlet fluid temperature and 3.2 lt/min flowrates results for 120 hours.

Unit heat transfer rates of BHEs drop rapidly below 0.25 kW/m after a few hours at the beginning of the test and it continues to decrease in 0.25-0.15 kW/m band until end of the test. It can be also clearly seen from there that all the BHEs have approximately the same unit heat transfer rates and thus can be said that they have almost the same thermal characteristics.

Experimental results of individual BHEs and obtained thermal conductivity values are given in detail in Wang et al, (2024).

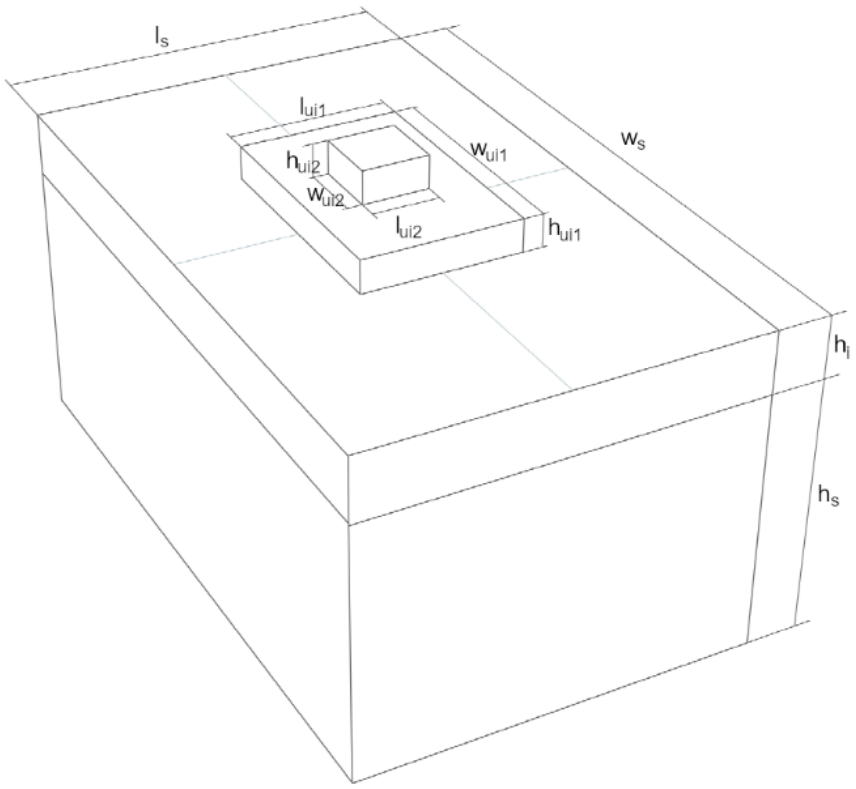

Fig. 3. 3D view of the storage field.

Because of technical problems in the test of BHE 2, the results cannot be presented in **Fig. 4**, however it is seen also that in the following sections that it has also same thermal characteristics with the others.

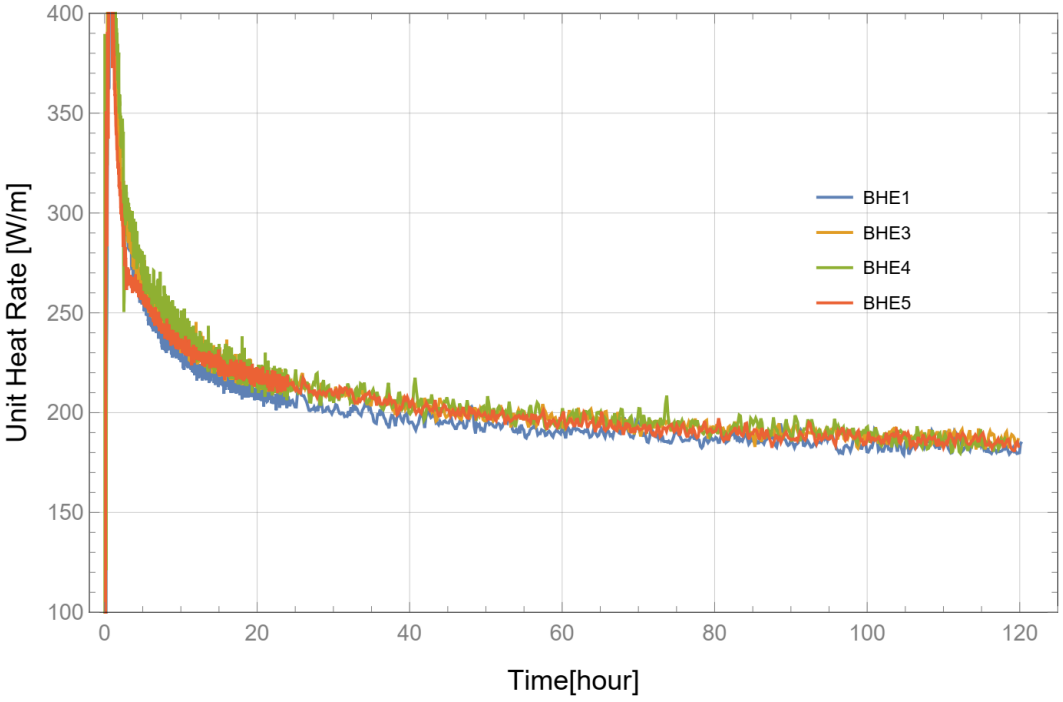

Fig. 4. Unit heat transfer rates of BHEs in each tests were carried out in different times.

Detailed geometrical properties of the storage field are given in **Table 4** .

Table 4. Geometrical properties of the storage field.

No	Name	Symbol	Value	
1	Depth of storage	h_s	200.0	cm
2	Depth of upper isolation	h_i	47.5	cm
3	Width of storage field	w_s	500.0	cm
4	Length of storage field	l_s	300.0	cm
5	Depth of top storage 1	h_{ui1}	25.0	cm
6	Width of top storage 1	w_{ui1}	90.0	cm
7	Length of top storage 1	l_{ui1}	60.0	cm
8	Depth of top storage 2	h_{ui2}	25.0	cm
9	Width of top storage 2	w_{ui2}	25.0	cm
10	Length of top storage 2	l_{ui2}	25.0	cm

Cyclic test results

In the cyclic tests, different time intervals were used to see the effect of time intervals in charge and discharge to the efficiency of tests. The sequence of the tests, total duration and number of charges and discharges are given in **Table 5**.

Table 5. Cyclic tests time plan

Test No	Name	Test Start	Test End	Total Duration	Charge	Discharge
1	48-h cycle	13.07.20 14:15	11.08.20 11:44	28.90 days	7	7
2	24-h cycle	12.08.20 18:00	23.08.20 18:00	11.00 days	6	5
3	12-h cycle	25.08.20 20:18	01.09.20 20:18	7.00 days	7	7
4	120-h cycle	02.09.20 14:00	14.09.20 10:42	11.86 days	1	1

In heating cycles, the flowrate was fixed to 16 lt/min in the main line and 3.2 lt/min in the BHE loops (Re=10961, in 70°C with ρ=977 kg/m^3 and υ=4.035x10^{-4} Pa.s) for cooling 4.1 lt/min in main line and 0.82 lt/min in BHE loops (Re=1008, in 15°C with ρ=999 kg/m^3 and υ=11.5x10^{-4} Pa.s) were used, flow regimes correspond to turbulence flow region for charge and laminar for discharge to provide. Discharge flowrates were limited with the pressure of the city grid and flowrate was chosen as a value that can be taken from the grid all day. Time intervals used for analysis were chosen as 48-hour, 24-hour, 12-hour and 120-hour to investigate effects of daily cycles. The cyclic tests were carried out in this sequence, however, in the last test (120-hour) because of technical problems only one charge and discharge could be completed.

48-24-12-hour 70-15°C cyclic test

Fig.5 a) shows inlet, outlet fluid temperatures and sand temperatures from different temperature sensors with different radial distances from the center in the A-transect for 48-24-12-hour tests. In the legend of the figure, the radial distance values from the center are also given. There X30 represents 5 cm radial distance from the center, and this corresponds to grout temperature of BHE 1, and it is notable here that the temperature reaches 60°C hardly after 48 hours and is not constant despite the fluid temperatures are constant. High and low inlet temperatures with different cycles produce a temperature profile like a square wave function in time scale. Instant changes of inlet temperature can be seen immediately inner part of the storage field, however wave packages of changes decay largely with distance as can be seen from the changes of temperature sensors P3.3, A6.6 and A7.6 in the same figure.

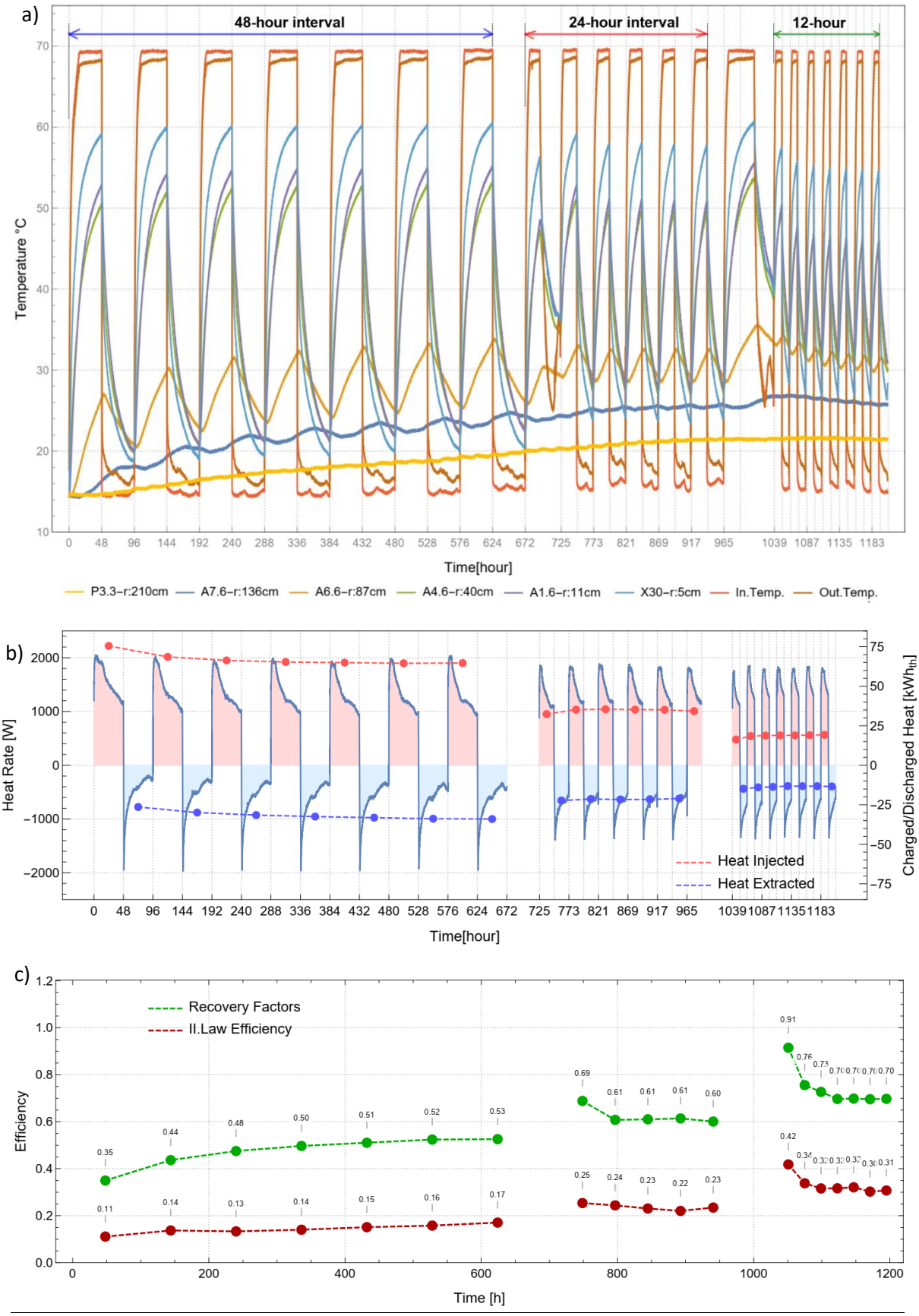

Fig. 5. a) Charge and discharge amounts from the cycles and recovery factors for 48-hour cyclic test. **b)** Injected heat and extracted heat amounts for 48-24-12hour cycle **c)** Recovery factors and II.Law efficiencies for the 48-24-12-hour cyclic tests.

24-hour test started immediately after 48-hour test and 12-hour cyclic test also started immediately after 24-hour cycle with the same test conditions. As can be seen the temperatures of the inner and outer part of the heat storage field are decreased and temperatures of the outer part is flatter than previous cycles, even though there is a very small decreasing trend. The temperature in the inner part decreases to 54 °C in the 24-hour cycle, it is 60°C in the 48h-cycle, and at A7.6 the temperature is around 26 °C and it increases slightly with time, however it starts to decrease slightly in the 12-hour cycle as well.

Fig.5 b) shows injected heat and extracted heat amounts for 48-24-12hour cycle. The temperatures and the flowrate are measured with 1 min intervals during the test and the heat transfer rates calculated with the following Eq.

$$\dot{q} = \rho_f C_{p.f} V_f \left(T_{in} - T_{out}\right) \tag{4}$$

As the number of cycles increases, the temperature of the ground also increases and extractable heat also increases. Total charged and discharged thermal energies can be found integral of the heat transfer changes with time:

$$q_{cyc} = \int_{t\_\text{cycle start}}^{t\_\text{cycle end}} \dot{q}(t)dt = \sum_{i=1}^{n} (t_{i+1} - t_i).(\dot{q}_{i+1} + \dot{q}_i)/2 \tag{5}$$

As is expected, heat transfer rates show high peaks at the change times of the shifts, i.e. at n x 48-24-12 h, n is the cycle lengths. Usage of interpolation function produces large errors because of peak points, therefore total thermal energy is calculated numerically with Eq.5 and they are given with large dots on the corresponding places in **Fig.5b.** The extracted and the injected heat energies are also given with dashed lines in the same figure.

Efficiency Calculations

For general efficiency evaluations of a storage system recovery rate that is based on the Thermodynamics' first law efficiency is used. Recovery rates of the cycles can be calculated with the following equation:

$$R_f = \frac{\text{Total extracted}}{\text{Total injected}} = \sum_{i=1}^{n} \dot{q}'_{cool} \Big/ \sum_{i=1}^{n} \dot{q}'_{heat} \tag{6}$$

The recovery rates and second law efficiencies are given in **Fig.5c**. In the first cycle the recovery factor is 0.35 and it increases continuously with cycles and after 6. cycle it becomes more stable in 0.52 with a slight increasing trend. This means that in the extracted energy in the discharge cycle is 52% of the injected energy during the charge cycle and this value also corresponds to first law efficiency for the used temperatures and flowrates. However, in this charge- discharge process charge temperature was 70°C and discharge temperature was mostly between 20-17°C (**Fig. 5a**), i.e high temperature that can be denoted high quality energy was injected to the storage field however low temperature that is relatively low quality was extracted in the process. The same amount of recovery factor can be also obtained with lower temperature heat energies and using only recovery factor for storage efficiency is not enough to totally determine the efficiency. Therefore, thermodynamics' second law efficiency (also exergy efficiency) can also identify efficiency of the cyclic charge discharge processes. The second law efficiency is equal to the ratio of the extracted heat exergy to the injected heat exergy:

$$\eta_{II} = \frac{X_{cool}}{X_{heat}} \tag{7}$$

for a heat transfer process, amount of exergy can be found with following equation (Dincer & Rosen, 2011)

$$X_{heat/cool} = \int \left(1 - \frac{T_0}{T}\right) \delta \dot{q} \tag{8}$$

where T_0 is the far field ground temperature and T is the inlet temperature for charging and return temperature for discharging.

As can be seen from **Fig.5c** the second law efficiency is quite lower than the recovery factors, after the first heat up duration, the recovery factor reaches to 0.5 however second law efficiency reaches only to 0.14. It means also that the quality of the injected energy is higher than the extracted energy, therefore storing the heat energy reduces the quality of energy. However, both efficiency values increase with the number of cycles.

It is remarkable also in **Fig.5c** that the recovery factors and second-law efficiencies in the 24-hour test are higher than the 48-hour. In this cyclic test it became stable around 0.60 however it was 0.52 in the 48-hour cyclic test, there is 15% increase, however the increment in the second law efficiency is around 37%.

The reason for this can be found from **Fig. 4**; in case of a constant temperature heat injection, heat transfer rates decrease by time (it is linear in log time scale for a single BHE) as can be seen from the heat transfer rate changes of heating cycles as given in **Fig. 5b**. The heat transfer rates decrease continuously during the heat injection and therefore, the first half of the heat injection cycles are higher than the latter part of the heat injections. This is also valid for cooling cycles as can be seen from the same figure.

Average temperature in the storage medium efficiency values based on the high and low temperature

Storage field temperatures from different times are interpolated with Kriging method (Davis, 1986) with using the temperature measurements given in the **Fig. 1** and illustrated in **Fig. 6**. The plots are also validated with numerical analysis (Lingenauer, J. 2020). Numerical modeling results including validating and further analysis would increase the pages of this manuscript, they are planned to be presented in another publication. In **Fig. 6** upper left figure shows temperature map of the field end of the discharge at 24.day, upper right shows 25.day after 24 hour heat charge, lower left is temperature map at 26.day after 48 hour heat charge and lower right is the map at 27.day after 24 hour discharge. It can be seen that the most of the temperature increase takes place at the first part of the heat charge and temperature decrease first part of the discharge.

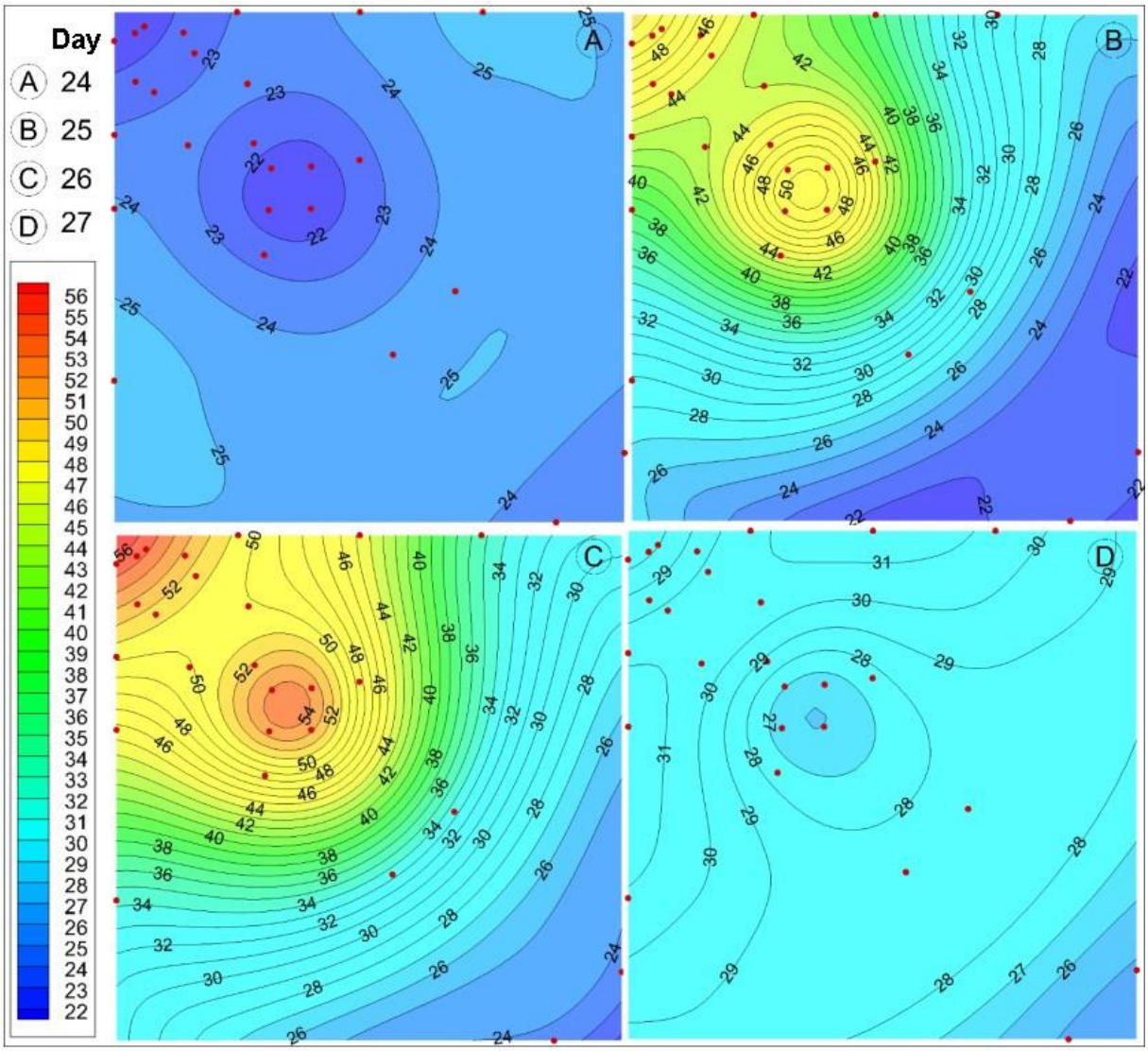

Fig. 6. Contour plots of interpolation of the measurements. A: Day 24 end of the discharge, B: Day 25 after 24-hour charge, C: Day 26 (after 48-hour charge), D: at day 27 after 24-hour discharge.

I.Law and II.Law efficiencies can be found at the end of the discharging process following a charge process, these values cannot describe current state of the storage field. However, in case of local temperatures are known in a storage volume, the current state of the storage field can be also calculated with the first law efficiency of heat accumulators as given by Bejan (2016)

$$\eta_I = \frac{E_{stored}}{E_{\max .stored}} = \frac{\rho V C_p \left(T - T_0\right)}{\rho V C_p \left(T_{high} - T_0\right)} \tag{9}$$

heat capacity of sand C_p does not change considerably in the test temperatures (Somerton, 1992) during the charge and discharge, then it can be simplified as following:

$$\eta_I = \frac{T - T_0}{T_{high} - T_0} \tag{10}$$

Here T_{high} is inlet temperature T_0 is initial and undisturbed temperature of the ground. T is the current temperature of the storage field. It is also average temperature of the volume, it can be calculated approximately analytically using the vertical temperature distribution (Hellström, 1991). However, in this study the temperature of the ground is measured more than 200 places, interpolated temperatures (**Fig. 6**) give more accurate results than the analytical approximation. In this case, by using the interpolation function T_i (x,y,z) average temperature can be find with following integration:

$$T = \int_V T_i(x,y,z)\,dV = \int_x \int_y \int_z T_i(x,y,z)\,\mathrm{d}x.\mathrm{d}y.\mathrm{d}z \tag{11}$$

To avoid the extrapolation, boundaries of the calculation volume are chosen related to dimensions of the farthest temperature sensors. For x-direction and y-direction the farthest sensor is P3.3 and for z-direction temperatures are measured from z=0, -5, -10, -30, -60, -100, -150 and -200 cm for AX and for BX, also 0, -30, -100 and -200 for PX.Y sensors. The integrated temperature area is depicted with red dashed box in **Fig. 1**. Obtained average temperature is given in **Fig. 7** with the temperature between BHEs, BHE1 - BHE3 and BHE3 – BHE2.

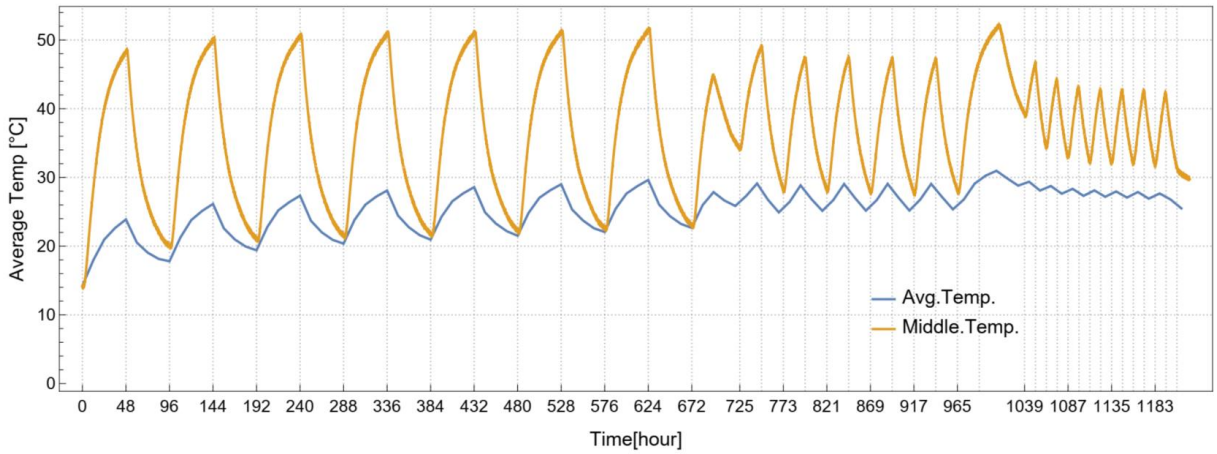

Fig. 7. State change of the storage field during the test.

And state of the storage field is obtained as given in **Fig. 8**, the average temperature of the storage is equal to initial ground temperature and the state of initial condition is 0 in the first charging cycle state of the storage reaches 18% and during the test maximum storage rate is 28%. The lower storage values are related to the number of BHEs with more BHEs higher storage values can be reached.

The current state of the storage volume is increased in the 48-hour cycle, however it stays constant in the 24-hour cycle and decreases in 12-hour cycle. If the first thermal build up stage the current state is increased higher rates than 28%, temperature gradient in radial is increased and heat loss to the uninsulated parts also is increased and the behavior of the storage field to the cycle length also changes. Therefore, heat loss from the storage volume is also important in the efficiency analysis.

Total injected heat to the storage field and heat Loss

If the average temperature of the storage field is known, total stored energy also can be found with following expression:

$$E_{stored} = \rho V C p\left(T - T_0\right) \tag{12}$$

and total injected energy is accumulation of the heat transfer rates given in **Fig. 5b** and Eq.4. and using Eq.5 for along the test.

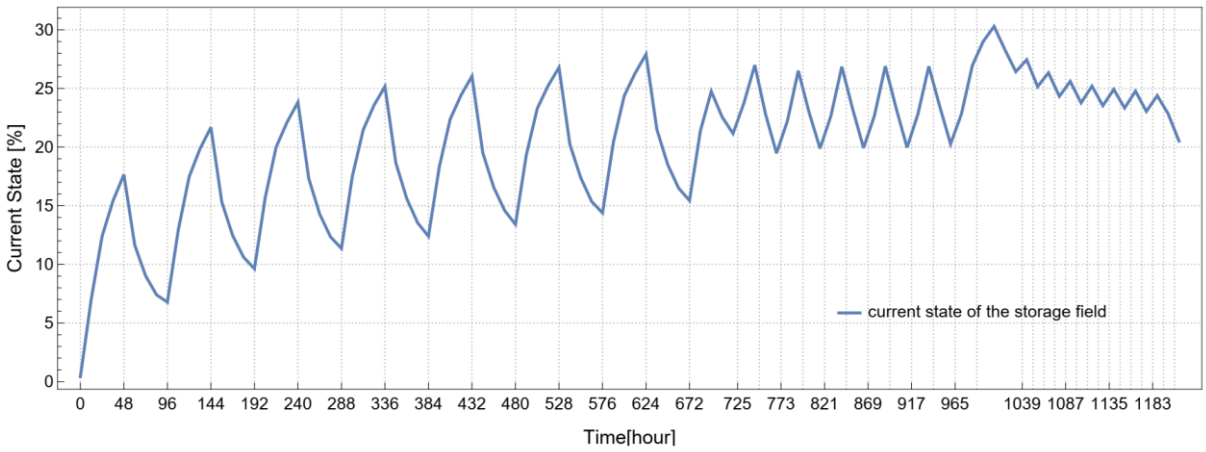

Fig. 8. Stored energy in the storage field and total injected energy to the field.

The results are given in **Fig. 9**, upper curve represent total injected heat energy to the storage volume and lower curve represents the stored energy in the volume. At the first heating cycle heat loss is minimum, therefore all the heat energy injected to the storage field is resulted increase of the stored energy in the field. However, after the first heating cycle, the temperature is propagated to the outer part of the storage and heat loss from the storage volume is started. Furthermore, the difference between $E_{\text{total injected}}$ and E_{stored} yields total heat loss from the storage volume $E_{\text{total heat loss}}$ as given following:

$$E_{\text{total heat loss}} = E_{\text{total injected}} - E_{\text{stored energy}} \tag{13}$$

It is also possible to validate thermal recovery factor of the storage system with the following equation (Dincer & Rosen, 2011):

$$R_f = 1 - \frac{E_{\text{total heat loss}} + E_{\text{stored}}}{E_{\text{total injected}}} \tag{14}$$

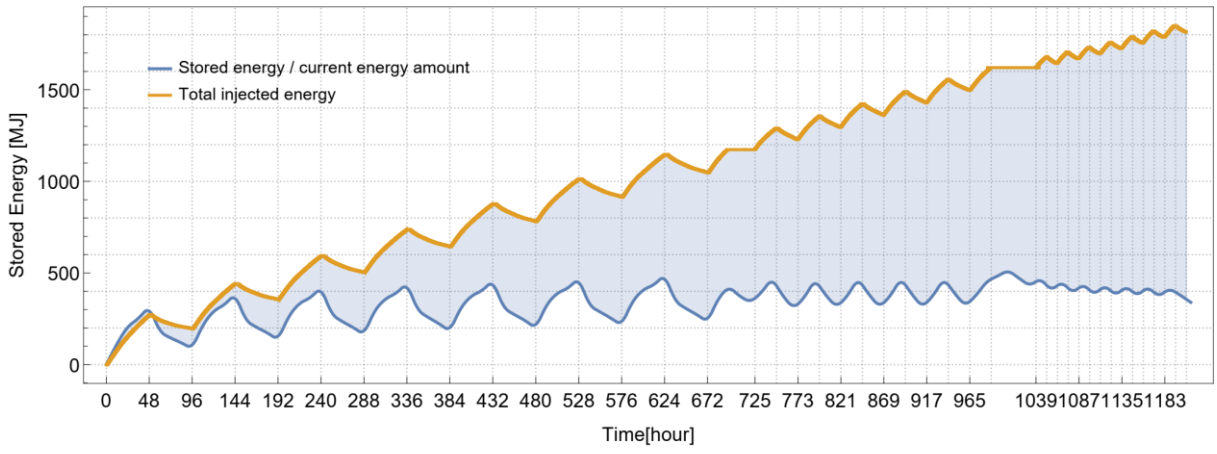

Fig. 9. Change of stored energy in the storage field and total stored energy during the tests.

Total heat loss is combined with heat loss from top and from the uninsulated ground/concrete interfaces:

$$Q_{\text{total heat loss}} = Q_{\text{top}} + Q_{\text{bottom}} + Q_{\text{lateral}} \tag{15}$$

The heat loss from the upper surface depend on air temperature and insulation thickness and can be calculated from the following Eq.

$$Q_{\text{top}} = \lambda_i \left(T_{\text{x, y, 0}} - T_{\text{air}}\right)\left(\frac{w_s l_s - w_{ui1} l_{ui1}}{h_i} + \frac{w_{ui1} l_{ui1} - w_{ui2} l_{ui2}}{h_i + h_{ui1}} + \frac{w_{ui2} l_{ui2}}{h_i + h_{ui1} + h_{ui2}}\right) \tag{16}$$

and from the lateral surfaces and from the bottom:

$$Q_{\text{lateral+bottom}} = \lambda_g \left(A_{\text{lateral-x}} \left.\frac{\mathrm{d}T}{\mathrm{d}x}\right|_{x=L} + A_{\text{lateral-y}} \left.\frac{\mathrm{d}T}{\mathrm{d}y}\right|_{y=w} + A_{\text{bottom}} \left.\frac{\mathrm{d}T}{\mathrm{d}z}\right|_{z=-h}\right) \tag{17}$$

Total heat loss and the heat loss from the top surface is given also in **Fig. 10**. The heat loss to the air is quite low in comparison with the total heat loss, that is around 300-330 W and it is interesting to see here from that heat loss in some days were reversed the direction, from the air to the field. The area between the two curves represent the heat loss to the surrounding ground. It can be also seen that after 18 days the heat loss is more stable, and a thermal balance was built between the storage volume and the surrounding ground based on the cycle length.

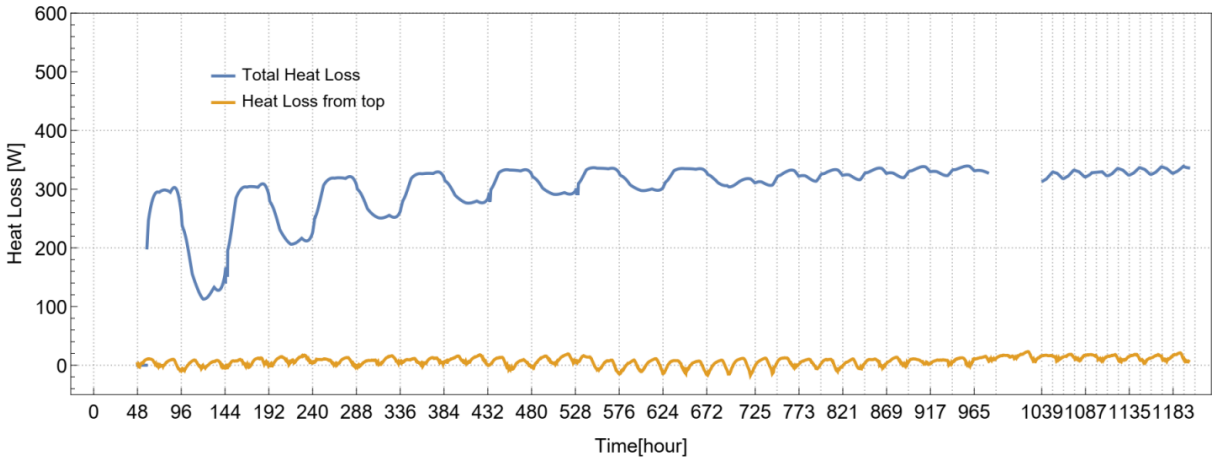

Fig. 10. Total heat loss from the storage volume and the heat loss from the top surface.

The thermal balance can be seen better in the r-z profile of the storage field as is presented in **Fig. 11**. After thermal balance building around the storage field, the temperatures stay almost constant. The temperature at 210 cm away stays at 22°C and at 136 cm it changes only between 22-26°C. It is also possible to predict from here that 330 W heat injection is adequate to keep the stored energy in the storage volume with the given conditions.

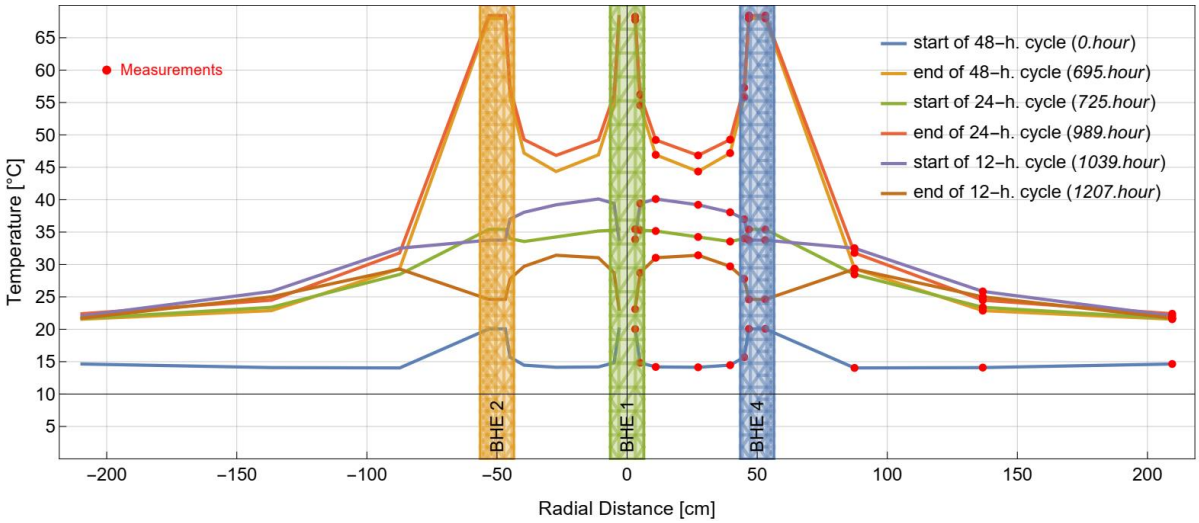

Fig. 11. Radial Temperature profile of storage field in A-transect in the cyclic tests.

So far between 48-hour and 12-hour cycle is investigated, and another question arises from here if the cycle length is longer what would the results change. For this reason, immediately after 12-hour cycle, cycle length was increased to 120 hours. The results are given below:

120-hour 70-15°C cyclic test and comparison of the results with the individual tests

In the last step, all BHEs were run together in same charge and discharge temperatures and flowrates for 120 hours. In this cycle a total of 118.8 kWh_{th} was injected and 59.7 kW_h was extracted and obtained recovery factor is 0.5, i.e. $\eta_I = 50$ % and second law efficiency is $\eta_{II} = 9.8$ % (**Fig. 12** and **Fig. 13**).

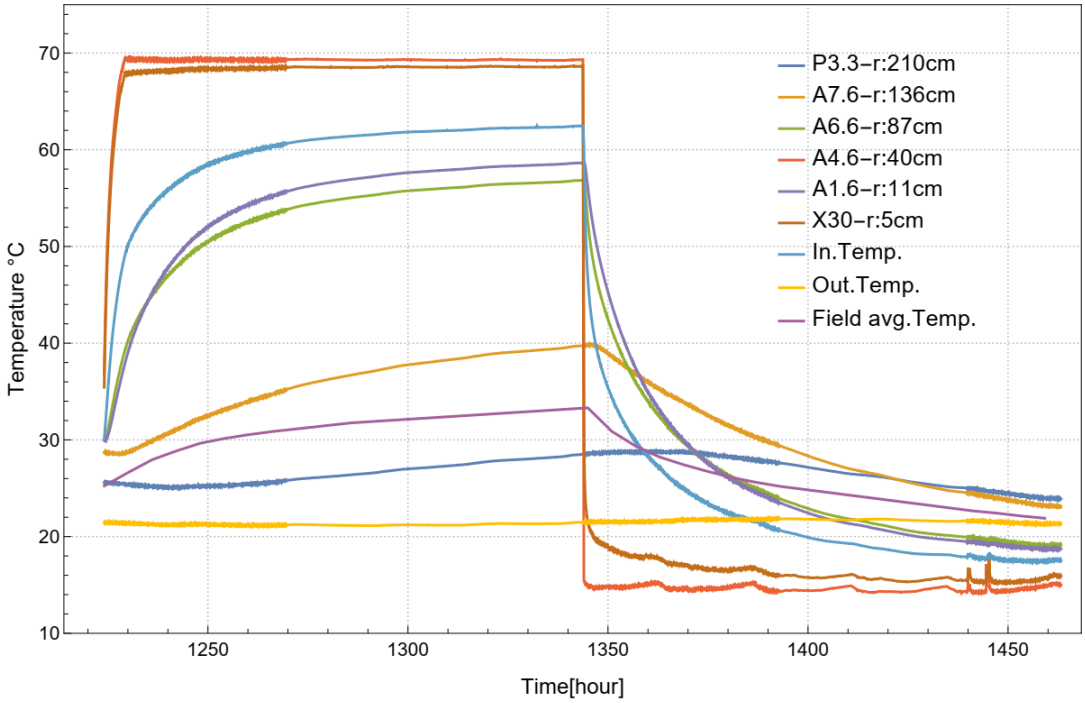

Fig. 12. 120-hour test temperatures and average temperatures.

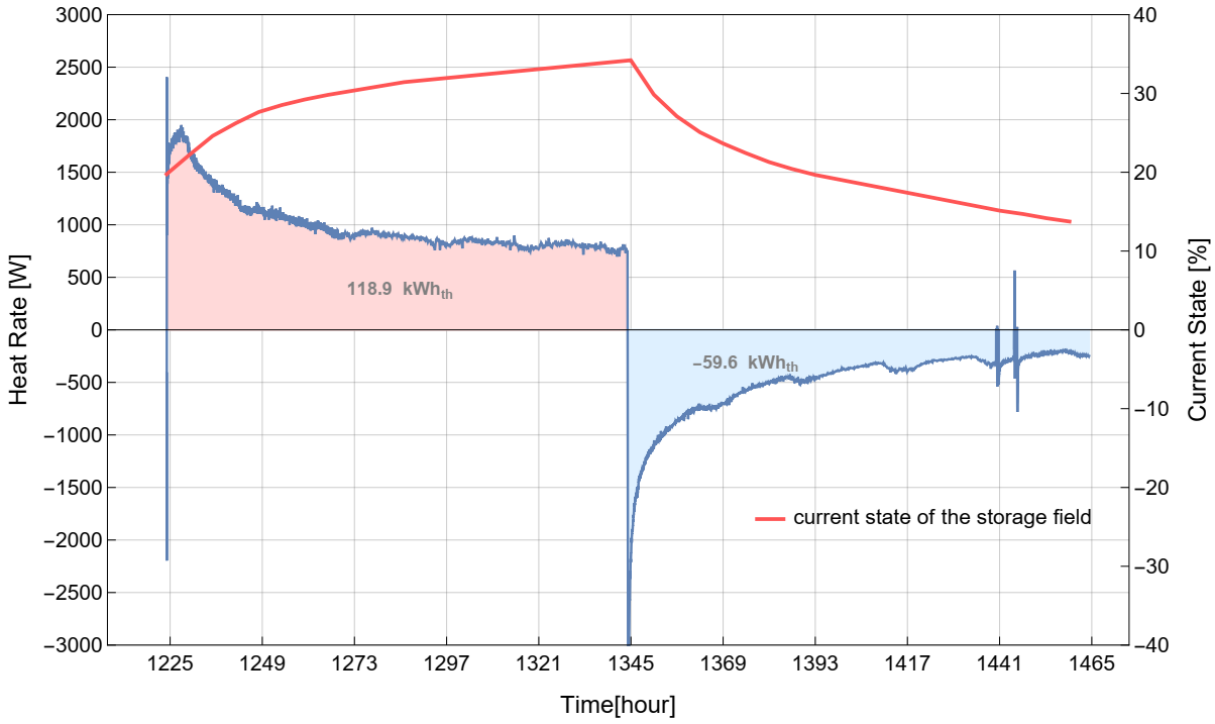

Fig. 13. Heat Transfer Rates and state of the storage for 120-hour test.

Total charged and discharged energies, recovery factors for all cyclic tests and their total and average values are summarized in **Table 6**.

Table 6. Summary of the charged and discharged heat energies and efficiencies of cyclic analysis.

		1.Cycle	2.Cycle	3.Cycle	4.Cycle	5.Cycle	6.Cycle	7.Cycle	Total/Avg
48 hour	Heat	74.6	67.7	65.5	64.5	64.1	63.7	63.8	**463.9**
	Cool	25.4	29.1	30.6	31.6	32.4	32.8	33.2	**215.1**
	Rf	0.34	0.43	0.47	0.49	0.51	0.51	0.52	**0.46**
	II.Eff.	0.11	0.14	0.13	0.14	0.15	0.16	0.17	**0.14**
24 hour	Heat	32.4	35.2	35.5	35.2	35.1			**173.4**
	Cool	22.3	21.4	21.6	21.6	21.1			**108.0**
	Rf	0.69	0.61	0.61	0.61	0.60			**0.62**
	II.Eff.	0.25	0.24	0.23	0.22	0.23			**0.23**
12 hour	Heat	16.3	18.5	18.8	18.9	18.9	19.0	19.3	**129.7**
	Cool	14.9	14	13.6	13.2	13.2	13.2	13.4	**95.5**
	Rf	0.91	0.76	0.72	0.70	0.70	0.69	0.69	**0.74**
	II.Eff.	0.42	0.34	0.32	0.32	0.32	0.30	0.31	**0.33**
120 hour (1cycle)	Heat				118.8				**118.8**
	Cool				59.7				**59.7**
	Rf				0.5				**0.50**
	II.Eff.				0.10				**0.10**

Table 7 shows an energy summary of 96-hour for 12, 24 and 48-hour cycles. During the 96-hour, for 48-hour cyclic test 1 charge and 1 discharge, for 24-hour cyclic test 2 charge and 2 discharge

and for 12-hour cyclic test 3 charge and 3 discharge cycles were completed. Because of being the first test, for 48-hour cyclic test last 96 hours data of the test was used. As can be seen from the table, the charged energies are close to each other however when the cycle interval decreases discharge energies increase. In the cycles approximate amounts of energy are injected that changes between 63.8 kWh_{th} and 72.5 kWh_{th} however, the extracted energy is 55.7 kWh_{th} for 12-hour cycle, that is 27% higher than 24-hour cycle and %68 higher than the 48-hour cycle. It is interesting to see here that with approximately the same amount of energy in same total time and same charge and discharge durations existed, and higher energy can be extracted with shorter cycle durations.

Table 7. Energy summary of 96 hour for different cycles.

Time	12	24	36	48	60	72	84	96	Charge	Discharge
48-hour	63.8				-33.2				63.8	-33.2
24-hour	32.4		-22.3		35.2		-21.4		67.6	-43.7
12-hour	16.3	-14.9	18.5	-14.0	18.8	-13.6	18.9	-13.2	72.5	-55.7

The reason can be seen also from **Fig. 14**, where the interpolated temperature contours of the field after 96.hour for 48-hour, 24-hour and 12-hour are illustrated. After 12-hour temperatures are between 26.3-32.8°C, for 24-hour 19.0-21.1°C and for 48-hour between 22.7-25.7°C. In the longer discharge case, the temperature of the field is dropped to very low temperatures than the other cycles. It is also can be observed from the middle ground temperature changes in **Fig. 15**. This indicates that in longer cycles the injected heat is propagated more wide area than the shorter steps and less heat can be extracted, however in shorter cycles the injected heat can be recaptured before it diffuses to the outer parts.

It can be thought that 48-hour cycle is the first test, 12-hour cycle is the last test, and because of that higher heat energies can be extracted. In **Table 8**, 24-hour cyclic test and 120-hour cyclic test are also compared. 24-hour cyclic test was earlier than the 120-hour cyclic test and as can be seen from the **Table 7** in 24-hour cycle 45% more energy injected, and 80% more energy extracted in same time and recovery factor 10% higher than the 120-hour cyclic test.

Table 8. Energy summary comparison of 24-hour and 120-hour cyclic tests.

Time	24	48	72	96	120	144	168	192	216	240	Charge	Discharge
		-		-		-		-		-		
24-hour	32.4	22.3	35.2	21.4	35.5	21.6	35.2	21.6	35.1	21.1	173.4	-108.0
120-hour	118.8					-59.7					118.8	-59.7

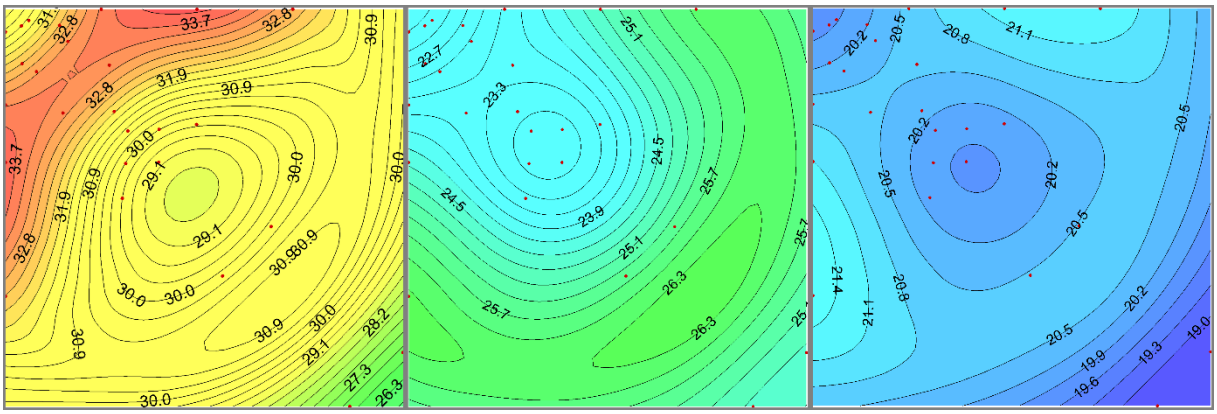

Fig. 14. Temperature contours after 96. hour running case considered in **Table 7**. a) for 12-hour cycle, b) for 24-hour cycle c) for 48-hour cycle (Lingenauer, 2020).

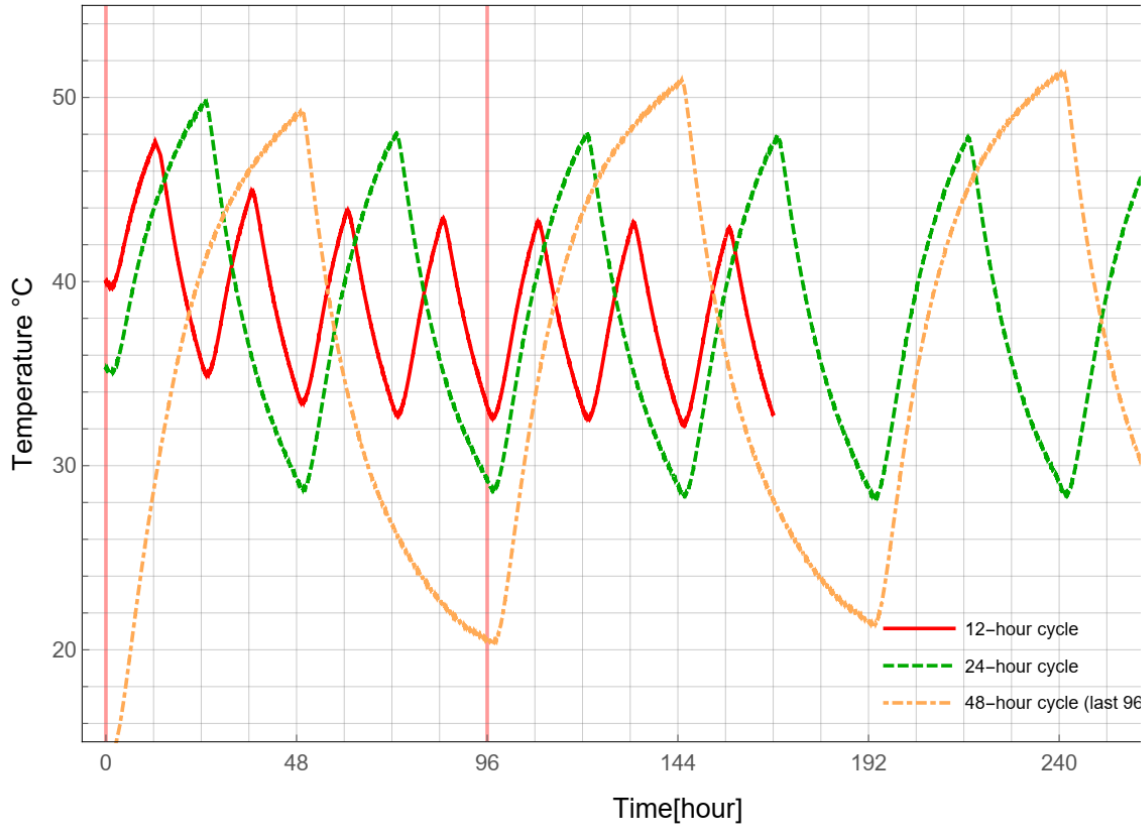

Fig. 15. Sand temperatures at the middle of the BHEs for different cycles.

Fig. 16 shows temperature distribution along the A-transect for alone and together working conditions. In x-axis 0 denotes the center of the storage field and to left and right sides represent radial distance from the center and the points are the corresponding sensor locations. At the center of the field, BHE1 exists and at right BHE 4 and at left BHE 2 are located. Upper curves in the **Fig. 16** are plotted using temperature measurements at different times. Lower curves indicate temperature changes with time for alone working conditions for the middle BHE (1). As the interaction test carried out in sequence of the cyclic tests the initial temperature is higher than the alone working condition. Nevertheless, from the figure it can be observed that the region between the boreholes can be easily heated up, however for alone working case temperatures decrease strongly with radial distance.

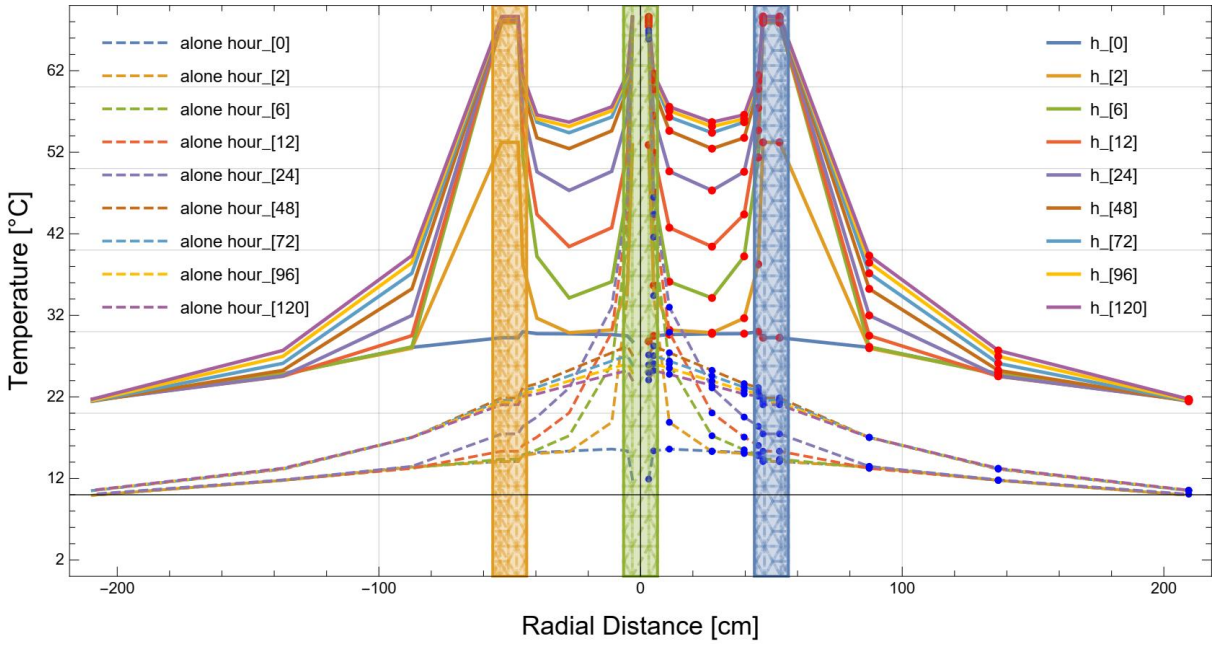

Fig. 16. Temperature distribution in A-transect in together and alone working conditions.

4. Discussion

Thermal recovery factor depends on many factors like charge - discharge energies, temperatures, geometry of the storage field (depth of BHEs, distance between BHEs, type of the BHE) and thermal and geologic properties of the storage material, isolation, other environmental factors air, groundwater, moisture, ground temperature and storage strategy (parallel, serial, circulation of the fluid inside the field) and quality of labor and instruction. Based on all these factors a storage field will have a stable recovery factor after a first starting phase. This value changes from 40% up to 70% in the real BTES systems (Bauer et al. 2010). However, only recovery factor is not enough to indicate quality of a storage system, second law efficiency and current average temperatures are also important indicators for comparison.

For longer cycles recovery factors are 0.46-0.5 (48-hour and 120-hour cycle) however second law efficiencies are only 0.14 and 0.10. The efficiency values obtained in this study are special to this storage field that is also related properties of the storage field and operating conditions, however in this study the storage system was run in different time interval cycles in different aims and change of outputs are observed. As can be seen from the cyclic analysis, recovery factor and second law efficiencies increase with decreasing of the time intervals when the other parameters are kept constant. In 12-hour cycle recovery factor reaches 0.70 and second law efficiency to 0.33 and more energy can be extracted. As has been seen also in the analysis, increasing of the time interval after some value does not affect much the magnitude of the thermal recovery factor. For 48-hour cycle recovery factor reached to 0.5 after 5-6 cycle, approximately the same recovery factor is also obtained for 120-hour cycle.

Another important factor in the running of a BTES system is middle temperature of the field. Inside the storage field, temperatures can reach higher temperatures very faster than the outer parts. Temperature at the middle of the BHE heats up quite fast until a certain time and after that it is slowed down.

However, as the storage system is small, the max. stored energy is also low. It lays around 400 MJ from **Fig. 9** and average temperature lays around 25 °C with 15°C initial temperature (**Fig. 7**), if

this energy is stored in a water tank, it corresponds to a 9.5 m^3 tank (V = 400.10^6 J / (998. kg/m^3 .4181 J/(kgK). 10 K)), with 2.5 m high 2 m diameter can be also employed. With 25°C inner temperature and 15 °C air temperature with 0.1 m isolation heat loss will be 131 W, that is less than half of the heat loss from the field as given **Fig. 10**.

In design processes, recovery factors can indicate practically how much energy recovered from the storage field, however second law efficiency rather can be used in design process. Higher second law efficiencies correspond high quality energy storage and in very early design of the system it provides a deciding factor for the designers. In an underground storage, heat is dissipated in wide areas and intensity of energy is lowered and low second law efficiencies are obtained however, storage in a tank keep the energy more intense area and higher second efficiencies can be obtained without losing the quality of the energy. In the comparison of two systems or two states it can be seen same recovery factors however second law efficiency might be different, therefore in comparison and in design both efficiencies provide better comprehension. To see instant changes and current state of the storage volume first law efficiency of the accumulators can be used with measuring temperatures of the volume from different points and finding the average temperature of the volume.

Conclusion

In this study thermal analysis of a meso-scale BTES system is carried out based on the recovery factors, second law efficiency and the average temperature of the storage field with cyclic test with different time intervals. The following points can be drawn:

- As the time intervals in the cycles decrease, higher efficiencies are obtained. Recovery factor is between 0.76 – 0.70 for 12-hour and 0.50 - 0.53 for 48-hour cycle, similar increment is seen also for the second law efficiency.
- Heat loss from the top surface is quite low in comparison with the lateral surfaces, even in some days direction of the heat transfer is also reversed. In the given analysis, the steady state heat loss is around 300 W, on the contrary heat loss from top surface barely reached 20 W.
- After thermal built up is developed, periodical charge and discharge is taken place in a limited volume, for the given conditions in this study with two months test, temperatures at 200 cm away from the center changed slightly.
- Therefore, meso-scale BTES systems can be employed to absorb periodical changes in charge and discharge by establishing a thermal balance between the surrounding ground like accumulation water tank that works as a buffer.

Acknowledgment

We gratefully acknowledge funding provided by the Federal Ministry for Economic Affairs and Energy, Germany (BMWi, Grant 0325547B) and the support of the Project Management Jülich, Germany (PTJ).

References

Abbas Z., Chen D., Li Y., Yong L., Wang R.Z. 2020. Experimental investigation of underground seasonal cold energy storage using borehole heat exchangers based on laboratory scale sandbox. Geothermics 87, 101837.

ASHRAE. ASHRAE handbook: HVAC applications. Atlanta, GA, USA: ASHRAE; 2011

Baser T. and McCartney J. S. 2020. Transient evaluation of a soil-borehole thermal energy storage system. Renewable Energy.

Bauer D., Marx R., Nußbicker-Lux J., Ochs F., Heidemann W., Müller-Steinhagen H. 2010. German central solar heating plants with seasonal heat storage. Solar Energy 84, 612–623.

Bayer P., de Paly M., Beck M. 2014. Strategic optimization of borehole heat exchanger field for seasonal geothermal heating and cooling. Applied Energy 136, 445-453.

Bejan A. 2016. Advanced Engineering Thermodynamics, 4. Ed. John Wiley and Sons, Ltd. Publication.

Davis J. C., Statistics and Data Analysis in Geology, Second Edition, John Wiley & Sons, New York, 1973, 1986.

Dincer I. & Rosen M. A., 2011. Thermal Energy Storage Systems and Applications 2nd Edition. John Wiley and Sons, Ltd. Publication.

Ekmekci E, Aydin M. Ozturk Z.F., Sisman A. 2024. Very high temperature BTES: A potential for operationally cost-free and emission-free heating. Applied Energy, 360, 122859.

Ekmekci E. Ozturk Z.F., Sisman A. 2023. Collective behavior of boreholes and its optimization to maximize BTES performance. Applied Energy, 343, 121208.

Gehlin S. 2016. Borehole thermal energy storage. In: Simon J. Rees, editor. Advances in ground-source heat pump systems. Woodhead Publishing. p295-327.

Giordano N. and Raymond J. 2019. Alternative and sustainable heat production for drinking water needs in a subarctic climate (Nunavik, Canada): borehole thermal energy storage to reduce fossil fuel dependency in off-grid communities. Applied Energy 252, 113463.

Guo F., Zhu X., Zhang J., Yang X. 2020. Large-scale living laboratory of seasonal borehole thermal energy storage system for urban district heating. Applied Energy 264, 114763.

Hellström G. 1991. Ground heat storage: thermal analyses of duct storage systems. PhD. Thesis. Lund University.

Kavanaugh S. and Rafferty K. 2014. Geothermal Heating and Cooling Design of Ground-Source Heat Pump Systems. 2014 ASHRAE.

Lanahan M., and Tabares-Velasco P. C. (2017): Seasonal Thermal-Energy Storage: A Critical Review on BTES Systems, Modeling, and System Design for Higher System Efficiency. Energies 10: 743.

Liedtke P. 2019. Design, Installation und Erstmessungen eines Testfeldes für geologische Hochtemperaturwärmespeicher im teilgesättigten Untergrund. MSc. Thesis. Institute of Geosciences, University of Kiel, Kiel, Germany.

Lingenauer J. 2020. Experimentelle Untersuchung thermischer Interaktionen an zyklisch betriebenen Erdwärmesonden. MSc. Thesis. Institute of Geosciences, University of Kiel, Kiel, Germany.

Lundh M. and Dalenbäck J.O. 2008. Swedish solar heated residential area with seasonal storage in rock: Initial evaluation. Renewable Energy, 33-4, 703-711.

Moradi A., Smits K. M., Lu N., McCartney, John S. (2016): Heat Transfer in Unsaturated Soil with Application to Borehole Thermal Energy Storage. Vadose Zone Journal 15 (10). DOI: https://doi.org/10.2136/vzj2016.03.0027

Naicker S.S., Rees S.J. 2020. Long-term high frequency monitoring of a large borehole heat exchanger array. Renewable Energy, 145, 1528-1542.

Nilsson E. 2020. Borehole Thermal Energy Storage Systems for storage of industrial excess heat, Performance evaluation and modeling. Linköping University Licentiate Thesis.

Nordell B. 1994. Borehole heat store design optimization. PhD. Thesis, Lulea University of Technology, S-971 87 Lulea, Sweden.

Nordell B., Snijders A. and Stiles L. (2015) The Use of Aquifers as Thermal Energy Storage (TES) Systems. Advances in Thermal Energy Storage Systems. Woodhead Publishing.

Pallard W.M., Lazzarotto A., Sequera J.A. Palm B. 2020. Design methodology for laboratory scale borehole storage: An approach based on analytically-derived invariance requirements and numerical simulations. Geothermics 87, 101856.

Rapantova N., Pospisil P., Koziorek J., Vojcinak P., Grycz D., Rozehnal Z. 2016. Optimisation of experimental operation of borehole thermal energy storage. Applied Energy, 181, 464-476.

Reuss M. 2015. The use of borehole thermal energy storage (BTES) systems, in Advances in Thermal Energy Storage Systems, Methods and Applications, Editor Luisa F. Cabeza.

Sanner B. and Stiles L., 1997. Status of seasonal cold storage in ground source heat pumps. In:Proc. The 7th International Conference on Thermal Energy Storage Megastock'97. June 18-21, 1997. Sapporo, Japan, pp. 13-18.

Sarbu I. and Sebarchievici C. 2018. A comprehensive review of thermal energy storage. Sustainability, 10, 191; doi:10.3390/su10010191.

Schulte D. O., 2016. Simulation and optimization of medium deep borehole thermal energy storage systems. Ph.D. thesis. Technische Universität Darmstadt.

Sibbitt B., McClenahan D., Djebbar R., Thornton J., Wong B., Carriere J., Kokko J. 2012. The Performance of a High Solar Fraction Seasonal Storage District Heating System – Five Years of Operation. Energy Procedia, 30, 856-865.

Siegenthaler J. (2011). *Modern Hydronic Heating: For Residential and Light Commercial Buildings*. Cengage Learning.

Skarphagen H., Banks D., Frengstadt B. S., Gether H. 2019. Design Considerations for Borehole Thermal Energy Storage (BTES): A Review with Emphasis on Convective Heat Transfer. Hindawi Geofluids, Vol.2019 A.ID:4961781, https://doi.org/10.1155/2019/4961781.

Somerton W.H. 1992, Thermal properties and temperature-related behavior of rock/fluid systems, Elsevier, New York, A.B.D.

ThermoCem® TC04 (2017): Technical Data Sheet. 60_thermocem_tc04_englisch.pdf?download=1. (20.12.2020) https://www.heidelbergcement.de/system/files_force/assets/document/7a/32/tds_3

VDI 4640, 2001. Thermiscche Nutzung des Untergrunds – Grundlagen, Gehenmigungen, Umweltaspekte. VDI Richtlinien.

Wang B., Beyer C., Aydin M., Bauer S. (2024). Experimental and numerical investigation of thermal interactions between high-temperature borehole heat exchangers in unsaturated and low permeable soil. Applied Thermal Engineering 248 (1), 123184 https://doi.org/10.1016/j.applthermaleng.2024.123184

Welsch B., Völker-Göllner L., Schulte D.O., Bär K., Sass I., Schebek L. 2018. Environmental and economic assessment of borehole thermal energy storage in district heating systems. Applied Energy, 216, 73-90.

Welsch B. 2019. Technical, Environmental and Economic Assessment of Medium Deep Borehole Thermal energy storage systems. PhD. Thesis, Technische Universität Darmstadt.